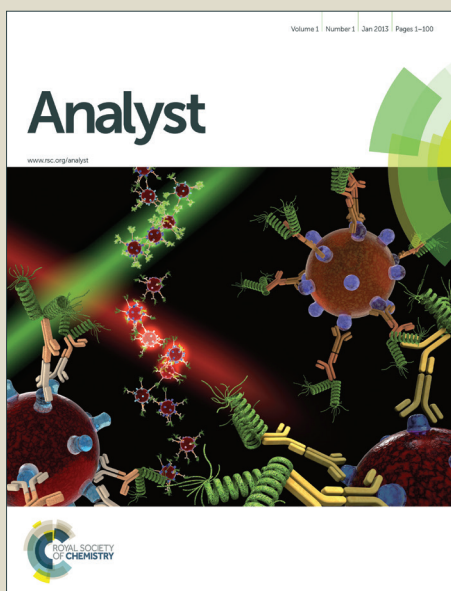


Analyst

Accepted Manuscript



This is an *Accepted Manuscript*, which has been through the Royal Society of Chemistry peer review process and has been accepted for publication.

Accepted Manuscripts are published online shortly after acceptance, before technical editing, formatting and proof reading. Using this free service, authors can make their results available to the community, in citable form, before we publish the edited article. We will replace this *Accepted Manuscript* with the edited and formatted *Advance Article* as soon as it is available.

You can find more information about *Accepted Manuscripts* in the [Information for Authors](#).

Please note that technical editing may introduce minor changes to the text and/or graphics, which may alter content. The journal's standard [Terms & Conditions](#) and the [Ethical guidelines](#) still apply. In no event shall the Royal Society of Chemistry be held responsible for any errors or omissions in this *Accepted Manuscript* or any consequences arising from the use of any information it contains.

Characterisation of a micro-plasma for Ambient Mass Spectrometry Imaging

Andrew Bowfield,^{*a,b} Josephine Bunch,^b Tara L. Salter,^b Rory T. Steven,^b Ian S. Gilmore,^b Dave A. Barrett,^c Morgan R. Alexander,^c Kirsty McKay^a and James W. Bradley^a

TABLE OF CONTENTS

Fig. 1 A schematic of the plasma device with labelled components.

Fig. 2 A typical negative ion mass spectrum of the PTFE substrate in the m/z 200 – 500 spectral window.

Fig. 3(a) Variation of average TIC and peak intensity of the m/z 297 ion from PTFE as a function of capillary diameter.

Fig. 3(b) A 2D contour map to show the average TIC as a function of gas flow for each value of r for a 56 μm diameter capillary.

Fig. 3(c) A 2D contour map to show the average TIC as a function of gas flow for each value of r for a 20 μm diameter capillary.

Fig. 4(a) Line profile of the intensity variation of the m/z 297 PTFE ion across a step edge for 30 μm , 43 μm and 56 μm diameter capillaries.

Fig. 4(b) Line profiles of the intensity variation of the m/z 297 ion across a PTFE step edge for a 22 μm diameter capillary at $z = 1$ mm, $r = 1.5$ mm and $z = 2$ mm, $r = 4$ mm.

Table 1. A table to show the source flow rate and spatial resolution of the line profiles contained in Fig. 4(a).

Table 2. A table to show the spatial resolutions of the line profiles contained in Fig. 4(b).

Fig. 5(a) Variation of spatial resolution as a function of gas flow for two different diameter capillaries at $r = 2$ mm and $z = 1.5$ mm.

Fig. 5(b) Variation of spatial resolution as a function of r and z for a 20 μm diameter capillary at 65 ml/min.

Fig. 5(c) Plot of the spatial resolution achieved with each capillary.

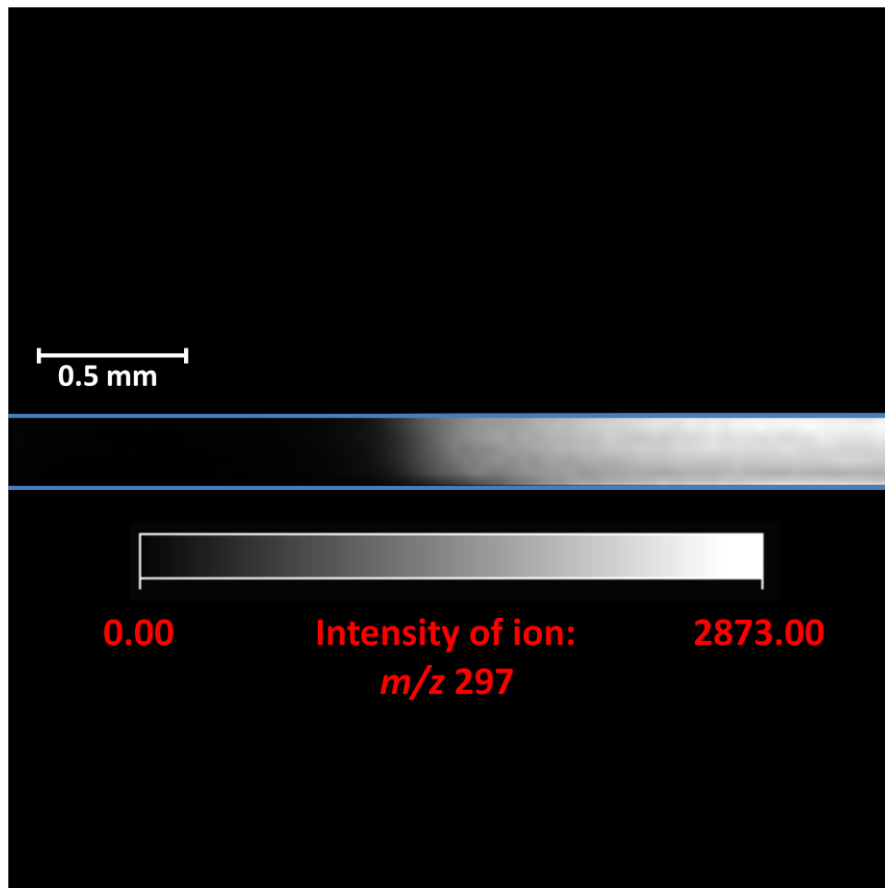
Fig. 6(a) An optical image of two halves of different cardamom seeds.

Fig. 6(b) Positive ion MS image of the seeds shown in Fig. 6(a) using the variation in intensity (counts) of the ion at m/z 81.

Novelty:

A systematic characterisation and optimisation of parameters of a plasma-mediated ion source to achieve the best spatial resolution for MSI.

Colour Graphic



Characterisation of a micro-plasma for Ambient Mass Spectrometry Imaging

Andrew Bowfield,^{*a,b} Josephine Bunch,^b Tara L. Salter,^b Rory T. Steven,^b Ian S. Gilmore,^b Dave A. Barrett,^c Morgan R. Alexander,^c Kirsty McKay^a and James W. Bradley^a

Received (in XXX, XXX) Xth XXXXXXXXXX 20XX, Accepted Xth XXXXXXXXXX 20XX

DOI: 10.1039/b000000x

Results are presented on the characterisation and optimisation of a non-thermal atmospheric pressure micro-plasma ion source used for ambient mass spectrometry imaging. The geometry of the experiment is optimised to produce the most intense and stable ion signals. Signal stabilities (relative standard deviation) of 2.3 – 6.5% are achieved for total ion current measurements from chromatograms. Parameters are utilised to achieve MS imaging by raster scanning of PTFE/glass samples with a spatial resolution of $147 \pm 31 \mu\text{m}$. A systematic study of resolution as a function of acquisition parameters was also undertaken to underpin future technique development. Mass spectra are obtained from PTFE/glass sample edges in negative ion mode and used to construct images to calculate the spatial resolution. Images are constructed using the intensity variation of the dominant ion observed in the PTFE spectrum. Mass spectra originating from the polymer are dominated by three series of ions in a m/z spectral window from 200 – 500 Da. These ions are each separated by 50 Da and have the chemical formula $[\text{C}_2\text{F} + [\text{CF}_2]_n]^-$, $[\text{CF} + [\text{CF}_2]_n + \text{O}]^-$ and $[\text{CF} + [\text{CF}_2]_n + \text{O}_3]^-$. The mechanism for the generation of these ions appears to be a polymer chain scission followed by ionisation by atmospheric ion adduction. Positive and negative ion mode mass spectra of personal care products, amino acids and pharmaceuticals, dominated by the proton abstracted/protonated molecular ion, highlight the potential areas of application for such a device. Further to this end a mass spectral image of cardamom seeds, constructed using the variation in intensity of possible fragments of the 1,8-cineole molecule, is included to reveal the potential application to the imaging of foods and other biological materials.

Introduction

The increasing importance of ambient ionisation mass spectrometry (ambient MS)^{1,2} as a tool for surface analysis and spectral imaging is unsurprising when one considers the number of successful applications in many areas of such a powerful technique. Recent studies have revealed applications including pharmaceuticals,^{3,4} polymers,^{4,5} micronutrients,⁶ drugs of abuse,⁷ agrochemicals in food stuffs⁸ and personal care products.⁹ While desorption electrospray ionization (DESI) was the first of these techniques,¹⁰ there are now a vast number of differing ion sources utilised in the field. Within this growing domain, plasma-based desorption and ionisation techniques¹¹ have developed as one of the leading variants.

Direct analysis in real time (DART),¹² established in 2005 and now commercially available, is currently the most common plasma-mediated ambient ion source. However, dielectric barrier discharge ionization (DBD)¹³ and low temperature plasma (LTP)¹⁴ (an annular version of DBD) are increasingly being utilised for ambient MS. These have the benefit of being inexpensive and easy to construct with the potential for rapid and on-site analysis when coupled to mobile mass spectrometers.^{15,16} Many other plasma sources have also been designed and tested successfully when combined with ambient MS.^{2,4,11}

The plasma afterglow is allowed to directly interact with the sample when using LTP, in common with plasma assisted desorption ionisation (PADI).¹⁷ Mechanisms proposed to explain the complex plasma chemistry apparent in each ambient ionisation source include direct electron impact ionization, metastable Penning ionization and ion-molecule interactions.¹⁷ Elucidation of such mechanisms has been aided by optical emission spectroscopy, especially for LTP,¹⁸⁻²¹ and molecular beam mass spectrometry.²² Most ambient plasma-based techniques employ helium as the discharge gas³⁻⁹ since the metastable ions produced by the breakdown processes contain a large amount of internal energy (He^* , $^3\text{S}_1$, 19.8 eV) which can directly ionise analytes through Penning ionisation. Also, the ionised He dimer, He_2^+ , has been identified as the dominant positive ion in this scenario and acts as an energy carrier into the plasma afterglow where charge is transferred to atmospheric nitrogen.^{18,19} This leads to the formation of N_2^+ , which is key in the creation of water clusters and hence proton transfer to the surface. While logic would suggest that different excitation processes in the various plasma devices may alter the dominance of primary mechanisms through which desorption/ionisation occur, a previous study²³ compared DART to both DBD and RF glow discharges and concluded that desorption/ionisation processes appeared to be indistinguishable between the three sources in the specific case of the ambient MS analysis of acetaminophen.

The device used in the current study is based upon the DBD/LTP construction due to the inherent non-thermal nature of plasma generation. These devices generate a highly nonequilibrium plasma through the formation of 'plasma bullets'. These 'bullets' are regions constituted of ions and vacuum ultra violet (VUV) photons²⁴⁻²⁶ ejected from the capillary when the applied voltage crosses a certain threshold in both the negative and positive regions of the voltage waveform. Initiation of the bullets is localised between the driven and ground electrode within the capillary volume and they are formed and ejected with a FWHM in the μs region.²⁶ This behaviour is displayed in Fig. S1 in the Supporting Information (SI) by the spikes in the current trace of the *IV* graph. The discrete packets act as the major vehicle for energy delivery to the surface and as such effectively create a non-continuous plasma, limiting the temperature within the capillary to approximately 60°C. While higher gas temperatures result in more efficient analyte desorption,^{8,23} the investigations herein avoid the use of such mechanisms in order to localise the incident plasma.

Investigations employing ambient plasma ion sources have primarily focused on applicability to a wide range of surfaces and molecules. Such efforts would be aided by a reduction in desorption footprint and associated improvement in spatial resolution to open up the field of ambient MS imaging analysis to such devices. Of the ambient techniques, currently DESI is the most widely used to obtain such images with a spatial resolution of 35 μm recently being achieved.²⁷ However, LTP²⁸⁻³¹ and PADI have the potential to operate in an imaging mode with improvements in design. At present, the best reported spatial resolution for plasma-mediated ambient MS is approximately 200 μm using LTP,³¹ where the device was used exclusively for sample removal. Although this is behind the resolutions routinely achieved in matrix-assisted laser desorption ionization (MALDI)^{32,33} or secondary ion mass spectrometry (SIMS),³⁴ those techniques require either complex sample preparation in the case of MALDI or vacuum conditions when referring to the latter. Studies using laser ablation

1
2
3 sources combined with plasmas have also produced images with spatial resolutions between 1 – 20 μm .^{35,36} The advantages
4 of using this alternative LTP over the techniques mentioned above are; the lack of complex or time consuming sample
5 preparations/procedures; the absence of solvents means there is no source of analyte de-localisation as in DESI; mass spectra
6 are dominated by the proton abstracted/protonated molecular ion;^{4,37} the ability to be used with analytes of any surface in the
7 absence of thermal damage;⁸ the control of fragmentation processes;¹⁴ its inexpensive design, construction, power
8 consumption and implementation coupled to its low source flow rates also result in a hugely important application of on-site
9 analysis with a truly mobile ion source. These advantages must be balanced against better spatial resolution in other
10 techniques, however, this technique provides complementary and orthogonal information to that obtainable by the other
11 techniques in a much quicker time-scale and at substantially lower cost (in comparison to expensive to maintain vacuum and
12 laser instruments.)
13
14
15

16 In this study, the authors develop a strategy of characterisation and optimisation of crucial operating parameters to
17 understand their impact on the spatial resolution of a non-thermal micro-plasma device. Not only do these investigations aid
18 in establishing the desired conditions in which mass spectrometry imaging (MSI) can be achieved with the best spatial
19 resolution, they also provide the basis for future technique development through a systematic experimental approach.
20
21
22
23
24
25
26
27
28
29
30
31
32
33
34
35
36
37
38
39
40
41
42
43
44
45
46
47
48
49
50
51
52
53
54
55
56
57
58
59
60

Experimental

Samples

Polytetrafluoroethylene (PTFE) was analysed in bulk form as thread-seal tape (RS, Corby, UK) which was wrapped around a standard glass microscope slide to present a uniform and flat surface to the ion source and replaced following each experiment to ensure no repeat sampling. Previous investigations^{4,5} have revealed the sensitivity of this polymer to plasma ion sources, hence it was chosen to probe the spatial resolution of the micro-plasma as a model system. 5 μ L of 10 mM pure components of personal care products (pcps) (liquids – triethanolamine, linalool, propylene carbonate) (Alfa Aesar, Heysham, UK) were deposited onto glass microscope slides and MS analysis conducted while wet. 5 μ g crystalline solids including amino acids (valine, leucine, phenylalanine), Fmoc (fluorenylmethyloxycarbonylchloride-pentafluoro-L-phenylalanine), caffeine (Sigma, Poole, UK), the phospholipid dipalmitoylphosphatidylcholine (DPPC) (Avanti Polar Lipids, Alabaster, AL, USA) and over the counter generic drug compounds ibuprofen and paracetamol, were also placed on glass slides for MS analysis.

Micro-plasma

The device is similar to the LTP,¹⁴ however the driven and earthed electrodes are reversed in this configuration.³⁸ An optical image of the micro-plasma in operation with the major components labelled can be found in the *SI* (Fig. S2) while a schematic is also included in Fig. 1. The experimental set up consists of a TG2000 function generator (AIM-TTI), operating at 14.25 kHz, driving a commercial audio amplifier (Crown Audio Inc., Indiana, USA, XLS 1000), with a voltage step-up transformer (Express Transformers & Controls Ltd, Runcorn, UK) at the output stage to generate the high ac voltages required for gas breakdown. Also connected at this point is a high voltage probe (Testec) whose output is read using an oscilloscope. The peak-to-peak voltage was set at 9.8 kV for all experiments. The device consists of a copper rod, 1.0 mm diameter, placed coaxially within a tapered borosilicate glass capillary 112.5 mm in length, 3.0 mm outer diameter and 1.6 mm inner diameter. The tapered end of these interchangeable capillaries is 10 mm in length and reduces to a diameter in the range 20 – 56 μ m (D_c) as specified by the manufacturer (C M Scientific Ltd, Silsden, UK). The copper rod acts as the driven electrode and is sharpened at one end. The sharpened tip of the rod is placed 11 mm from the end of the capillary to ensure the plasma is able to exit unhindered. Aluminium tape, 10 mm in width, is wrapped around the capillary 12 mm from the end and is electrically grounded. Helium gas, 99.996% pure (BOC, Guildford, UK), enters through a PTFE fitting, where it subsequently flows between the driven electrode and capillary and out through the tapered end. The helium flow rate is controlled via a rotameter (Omega engineering, Manchester, UK), and gas flow was varied in the range 5 – 65 ml/min.

Mass Spectrometer

A Thermo Scientific LTQ-Orbitrap Velos mass spectrometer (LTQ linear ion trap, nominal mass resolution) was used for all MS studies, unless otherwise stated. Negative ion mode MS was employed for all studies of PTFE as desorption/ionisation is not observed from this substrate in positive ion mode.⁵ Preliminary studies of PTFE established that the spectrometer needed to be programmed with a set ion trap injection time of 600 ms with automatic gain control turned off and 5 co-added micro-scans per spectrum. Total ion current (TIC) intensities were generated by summing ion signal intensity over the range m/z 200 – 500. The standard ion transfer tube was replaced with an extended version 127 mm in length (internal diameter 0.5 mm), but with the final 18 mm bent at an angle of 15 degrees towards the 2-axis stage. This tube is referred to as the ‘sniffer’ and the temperature was set to 225°C while held at a voltage of 0 V. All samples were placed on a 2-axis stage (Prosolia, IN, USA) 0.5 mm below the sniffer. The effect of the position of the device on the observed negative ion intensity from PTFE was investigated by recording TIC as a function of four parameters: the diameter of the capillaries at the nozzle exit (D_c), sniffer/capillary separation (r , 1 – 11 mm), the vertical distance separating the surface and capillary (z , 1 – 2 mm) and source flow rate. The optimal parameter values deduced from these studies were then used to conduct MSI of PTFE/glass samples.

1
2
3
4
5
6
7
8
9
10
11
12
13
14
15
16
17
18
19
20
21
22
23
24
25
26
27
28
29
30
31
32
33
34
35
36
37
38
39
40
41
42
43
44
45
46
47
48
49
50
51
52
53
54
55
56
57
58
59
60

Volatiles/non-volatiles – Both positive and negative ion modes were used for studies involving pcps, amino acids and pharmaceuticals. Negative ion mode MS was used to study Fmoc and negative ion tandem MS of DPPC (collision induced dissociation energy of 25.00 eV) was used to aid phospholipid identification.

Positive/negative ambient ions – The time-averaged spectra were obtained on a Hiden Analytical HPR-60 MBMS with the exit of a 56 μm diameter capillary placed 4 mm from the entrance orifice of the MS and aligned with the centre of the sampling orifice (100 μm diameter) along the discharge axis and parallel to the axis of the instrument. The sampling time of the detector was set at 1s and a source flow rate of 0.25 ml/min was used. This instrument has a mass range of 0–1000 Da, a resolution of 0.02 Da and was used for these studies as it was specifically designed for analysis of atmospheric pressure plasmas.²²

Mass Spectrometry Imaging (MSI)

PTFE – All images of PTFE were produced by compiling the raw data (.raw, Thermo Scientific Xcaliber) into an image (Firefly, Prosofia) which was then read into BioMAP (v.3.7.5.5, Novartis). The line profiles in Fig. 3a were generated from two dimensional 443 x 26 pixel grids (pixel size 11 μm x 11 μm) where each row took 4.50 min to record with each pixel acquisition time taking 0.54 s. The x-y stage moved at a rate of 18.519 $\mu\text{m}/\text{s}$. The line profiles in Fig. 3b were generated from 75 x 6 pixel grids (pixel size 40 μm x 40 μm) where each row took 3.96 min with each pixel acquisition time taking 3.17 s. The x-y stage moved at a rate of 12.62. It is important to note that the x-y stage cannot move at a speed less than 10 $\mu\text{m}/\text{s}$. All efforts were made to limit the speed of the stage to as low a value as possible so as not to impact upon the RSD achieved with each image.

Cardamom – The dried seeds were purchased whole from a local supermarket and were cut in half through the sagittal plane using a scalpel. Two halves of different seeds were chosen so as to be non-symmetrical. The seeds were then placed, with their interiors facing upwards, on sticky tape which was wrapped around a glass microscope slide and secured in the 2-axis stage. This stage was then lowered to 2.5 mm below the sniffer to ensure the seeds could pass freely beneath the sniffer. The thickness of the seeds was approximately 2 mm and the plasma device was placed 1 mm above the surface of the seeds at $r = 1.5$ mm as this produced the most intense spectrum from the seed surface not dominated by ambient ions. The separation between the plasma device and the surface of the seeds was not constant across the recorded image due to the uneven nature of the surfaces themselves.

Intense ion signals (10^4) were detected in preliminary studies of cardamom seeds, likely originating from volatile organic compounds (VOCs). The MS was programmed to collect 3 co-added microscans per spectrum and 200 ms injection time which allowed a scan time of 0.72 s per pixel with each row taking 0.90 min to acquire due to the abundance of aromatic molecules. The x-y stage moved at a rate of 277.78 $\mu\text{m}/\text{s}$ and the MSI consists of a 75 x 50 pixel grid.

Comparison of Line Profiles

Line profiles are generated by calculating the average ion intensity of the m/z 297 ion in each column of pixels along the x-axis and normalising to the maximum ion intensity. This method reduces the two-dimensional pixelated image into a single line of averaged pixels from which the spatial resolution can be calculated.^{39,40} Spatial resolutions are initially calculated by measuring the 16-84% interval of the line profile of the intensity variation of the ion across the step edge between the PTFE sample and the glass slide. This measurement provides the value of 2σ of the Gaussian broadening observed at the edges of the ‘top hat’ function⁴¹ and then this value is multiplied by $\sqrt{2\ln 2}$ to provide the FWHM and therefore the spatial resolution of the device.

Spatial resolution measurements are confirmed by fitting the normal cumulative distribution function to the ‘S’ shaped line profile using the standard deviation calculated by the process defined above. It is important to emphasise that this is a theoretical spatial resolution defined, as it is, by the broadening of the line profile generated at the step-edge between the PTFE tape and the glass slide. These processes neatly capture and define variations in spatial resolution as a function of the operating parameters.

Results and Discussion

AMS of Volatile/Non-volatile Compounds

The ambient ions resulting from mixing of the plasma produced using this device with the surrounding air agree with the conclusions of optical spectroscopy studies¹⁸⁻²¹ that the helium discharge gas is crucial to the mechanisms underpinning creation and propagation of the plasma afterglow. The dominance of the N_2^+ ion when the mass spectrometer was operated in positive ion mode (Fig. S3a, (SI)), and an excess of oxygen, ozone and water clusters when operated in negative ion mode (Fig. S3b, (SI)) are clearly visible.

In order to establish that this device produces similar typical mass spectra observed previously with the LTP,³⁷ i.e. dominated by the proton abstracted/protonated molecular ion with little fragmentation making identification relatively simple, tables of the positive (Table. S1) and negative (Table. S2) ions detected using ambient MS of volatile pcps and less/non-volatile amino acids, caffeine, paracetamol and ibuprofen are included in the SI.

The negative ion mass spectra of the volatile pcps displayed series of ions with additional oxygen components which originate from plasma/air interactions (Fig. S3b). The analysis of PC(16:0/16:0) DPPC is the first negative ion tandem MS of an intact lipid using a plasma ion source that the authors are aware of.^{42,43} The dominant peak at m/z 795 corresponds to the ion $[M+NO_3]^-$. The excited gas and air mixture produces adduct formation and addition to the subject molecule which allows for definitive identification of the lipid in the absence of solvent based adduction. Such behaviour has been reported previously.¹⁶ This is a potentially important result in the field of bioanalysis and increases the impact of the studies contained herein. This feature also occurs for investigations of PTFE and Fmoc.

Optimisation of Plasma MS

The micro-plasma device, shown in Figs. 1 and S2, was orientated normal to the surface for all studies contained in this report so as to ensure the activated plasma plume profile presented to the substrate was symmetrical.

A typical negative ion mass spectrum of the PTFE substrate is displayed in Fig. 2. There are three major ion series apparent in the m/z 200 – 500 spectral window and these are labelled with the same icons as those used previously to identify each series.⁵ The icons correspond to ions in the series $[CF+[CF_2]_n+O]^-$ ($n = 4, 5...9$) (\blacktriangle), $[C_2F+[CF_2]_n+O_3]^-$ ($n = 4, 5, \dots 9$) (\blacksquare) and $[CF+[CF_2]_n]^-$ ($n = 3, 4, \dots 8$) (\star). The lack of ambient ions produced by plasma/air interactions coupled to the ability to sample a relatively large region of the spectrum where this plasma device results in desorption/ionisation from the PTFE provides a basis for direct comparison as major parameters are varied. For consistency across data sets and since the series of ions with the adduction of oxygen to a polymer chain was consistently the most dominant, the ion located at m/z 297 was chosen to track variations in ion intensity for all chromatograms and mass spectral images of PTFE.

Fig. 3a displays the variation in negative TIC and intensity of the ion located at m/z 297 from PTFE for 56 – 20 μm diameter capillaries. An intermittent and unstable ion signal was observed for capillaries with diameters less than 20 μm and consequently these results are excluded from the data shown here. Decreases in both TIC and peak intensity of several orders of magnitude are clearly observed as the capillary diameter is reduced. The error bars display ± 1 standard deviation of three measurements from samples which were replaced following each plasma exposure. The relative standard deviation (RSD) of TIC for the 56 μm diameter capillary is the largest of the set at 6.5%, whereas those for the three others vary between 2 – 4%. Such stability is a significant improvement on that reported previously when using PADI (7%)⁵ or LTP (16%)^{7,8} and is of vital importance in mass spectrometry imaging. It is likely that reducing the diameter of the capillaries reduces the rate and number of plasma/air interactions around the main stream of ions and photons and hence decreases the sampling area of the surface. This limits the effect of turbulence induced treatment of the surface and increases signal stability²⁵ (reduces RSD) until a threshold is reached where further reducing the diameter of the capillary leads to a loss of signal due to the limits of detection of the sniffer and the amount of surface material desorbed. Evidence for this is found in the fact that the largest diameter capillary produced the most fluctuating signal. The data presented here leads the authors to

1
2
3 conclude that this intensity balance occurs when using capillaries with diameters less than 20 μm for non-volatile samples
4 and helium as the discharge gas.
5

6 TIC is presented as a 2D contour map as a function of gas flow and sniffer/capillary separation, r , in Figs. 3b and
7 3c as r is increased from 1 mm to 11 mm for (b) 56 μm and (c) 20 μm diameter capillaries at $z = 1$ mm. The surface/capillary
8 separation, z , was kept at a constant 1 mm throughout optimisation studies (investigated later) in order to limit gas diffusion
9 considerations and its impact on desorption footprint. The source flow rate was reduced successively by 5 ml/min every 25
10 seconds at each value of r . There are again large decreases in TIC observed with both capillaries as the source flow rate is
11 reduced and r is increased. The most intense TIC is observed at $r = 2$ mm for both capillaries. This is due to the fact that at r
12 = 1 mm, there is direct sampling of the plasma afterglow by the sniffer which reduces plasma volume at the PTFE surface
13 for both capillaries (subsequent data recorded at $r = 1.5$ mm saw a restoration of the signal to the approximate level
14 previously observed at $r = 2$ mm). A comparison of Figs. 3b and 3c shows that the intensity distribution is much more
15 confined and centred at $r = 2$ mm and 65 ml/min when using the 20 μm diameter capillary. This difference highlights that
16 the smaller capillary is more sensitive to variations in gas flow than the larger capillary. Indeed, gas flows below 20 ml/min
17 produced no detectable signal. Consequently, it is recommended that a minimum source flow rate of 45 ml/min be used
18 when employing such small diameter capillaries.
19

20 The lack of a persistent ion signal from PTFE when using capillaries with diameters less than 20 μm can be
21 explained by the lower number of ions reaching the surface per unit time by capillaries of this size. It is entirely plausible
22 that desorption/ionisation is occurring, but it is simply below the detectable limit of this sniffer due to lower ion throughput.
23 Alternatively, it is also possible that the life time of the plasma bullets outside the capillary may be decreased significantly
24 when coupling small diameter capillaries to low gas flow.⁴³ If collisions between atmospheric molecules and the He gas
25 increase resulting in greater gas diffusion with these smaller capillaries, desorption/ionisation may be prevented. If one
26 conjectures that the plasma bullets have a radial cross section containing ionic species and VUV photons in the inner core
27 surrounded by an envelope of activated gas species,²⁴⁻²⁶ the increased interaction of this envelope with the walls of the
28 narrower capillaries reduces the concentration of such species surrounding the plasma bullet. Since this envelope also decays
29 with distance, lower concentrations may result in fewer plasma interactions upon the analyte per unit time when using
30 narrower capillaries, even at high source flow rate. The threshold beyond which the reduction in capillary diameter restricts
31 the number of activated species per volume per unit time to reach the surface and induce desorption/ionisation at a level
32 which the MS sniffer can detect appears to be 20 μm . It is also interesting to note that negative ion signals are still observed
33 as r is increased beyond 10 mm. This suggests that this set-up produces ions which are long lived and it is diffusion with
34 ambient air which reduces ion intensity, although added turbulence induced desorption/ionisation from higher source flow
35 rates also clearly contribute to the persistent ion signal as r is increased.
36

37 Excluding data points for a source flow rate of 5 ml/min and maximum source-interface gap of $r = 11$ mm, RSD
38 using the 56 μm diameter capillary decreased to 7.6% from 14.8%. Calculations for the 20 μm capillary result in a RSD of
39 6.5% excluding data points at 20 ml/min and $r = 11$ mm as compared to 16.3% RSD when included. These results again
40 confirm the sensitivity of the lower diameter capillary to source flow rate as RSD decreases relatively more than that of the
41 larger capillary when the signal recorded using lower rates of gas flowing through the capillary are excluded from the
42 calculation.
43

44 **MSI and Spatial Resolution Calculations**

45 The line profiles displayed in Fig. 3a were generated using (1) 30 μm , (2) 43 μm and (3) 56 μm diameter capillaries and
46 where x is the distance across the mass spectral image. Using the process as defined in the experimental section under the
47 heading of 'Comparison of Line Profiles', the spatial resolution of the line profiles in Fig. 3a are calculated to be (1) 230 μm ,
48 (2) 346 μm and (3) 550 μm for 40, 35 and 25 ml/min source flow rates respectively. These values are tabulated in Table 1.
49

50 One can clearly observe the increasing width of the Gaussian broadening at the PTFE step edge as the diameter of
51 the capillaries increases. Also displayed in the inset of Fig. 3a is the 'error', or subtraction of the model from the
52
53
54
55
56
57
58
59
60

1
2
3 experimental data. This subtraction remains below $\pm 10\%$ for the line profile using the $30\ \mu\text{m}$ capillary across width of the
4 image and confirms the suitability of smaller diameter capillaries for imaging purposes. It is also important to point out that
5 the largest divergence between the model and the line profile data is consistently when the plasma plume is 'fully' on the
6 PTFE surface, as shown by the saturation of the cumulative distribution curve, and not on the positive slope of the intensity
7 profile.
8

9
10 Fig. 3b charts the direct comparison of two line profiles generated from images produced using a $22\ \mu\text{m}$ diameter
11 capillary where x is the distance across the $3\ \text{mm}$ mass spectral image. The position of the device changes from $z = 1\ \text{mm}$, r
12 $= 1.5\ \text{mm}$ to $z = 2\ \text{mm}$, $r = 4\ \text{mm}$ and is included to allow a direct comparison of the effect on the spatial resolution of the
13 position of the device. The spatial resolution of the dashed line is $145\ \mu\text{m}$ and increases to $497\ \mu\text{m}$ when the device is moved
14 further away from both the sniffer and the polymer (these values are tabulated in Table 2). A further point of note is that the
15 subtraction of the model from the experimental data (inset) lies almost exclusively in the $\pm 4\%$ range for the $r = 1.5\ \text{mm}$ data
16 set whereas that recorded at $r = 4\ \text{mm}$ displays much more variability over the -12 to 9% range as a function of x .
17
18

19 20 21 **Effect of Operating Parameters on Spatial Resolution**

22 It is important to measure the effect of the major operating parameters (r , z , D_c and source flow rate) on the spatial resolution
23 in order that optimisation studies fully consider parameter space. Such studies allow operating parameters to achieve the best
24 resolution to be stated with confidence (for this experimental system). Fig. 4a shows how spatial resolution varies as a
25 function of gas flow for 43 and $20\ \mu\text{m}$ diameter capillaries. The data presented in Fig. 4a is in good agreement with Fig. 2 as
26 it confirms the increased sensitivity of the narrower capillaries to gas flow. The sniffer/capillary separation, r , clearly has the
27 biggest impact on spatial resolution, as displayed in Fig. 4b, and is likely due to the greater diffusion of the desorbed PTFE
28 ions due to the longer sampling time and larger distances over which they have travelled. However, it is also significant that
29 the highest spatial resolution is achieved with the smallest values of z , r and D_c across both charts.
30

31
32 Fig. 4c shows the variation in the spatial resolution achieved for each different capillary. The spatial resolution has
33 been improved to $147 \pm 28\ \mu\text{m}$ by reducing the diameter of the capillary to $20\ \mu\text{m}$. Note that while the spatial resolution is
34 approximately linearly proportional to the capillary diameter, intensity (Fig. 2a) is approximately exponentially proportional.
35 The error bars show the RSD of the spatial resolution achieved with each capillary positioned at $r = 1.5\ \text{mm}$ and $z = 1\ \text{mm}$.
36 This position has been selected as the optimal position for the device after consideration of the data displayed in the previous
37 figures. A resolution of $147\ \mu\text{m}$ is a modest improvement to the current best spatial resolution achieved with plasma ion
38 sources³¹ ($200\ \mu\text{m}$) and is an important addition to the field of complex mass spectrometry imaging.
39

40
41 The limiting factor in terms of improving spatial resolution beyond $147\ \mu\text{m}$ appears to be the lack of a stable ion
42 signal when using capillaries with diameters below $20\ \mu\text{m}$ and sampling non-volatiles on different substrates, possibly due to
43 low volumetric gas flow. Studies are continuing with the current device to obtain images of a similar resolution to those
44 reported previously when using DESI.²⁷
45
46

47 48 **MSI of Cardamom Seeds**

49 Fig. 5a shows a $15 \times 10\ \text{mm}$ optical image of two different halves of freshly cut cardamom seeds (*Amomum subulatum*) An
50 inspection of Fig. 4c suggests the spatial resolution of the device at $r = 1.5\ \text{mm}$, $z = 1\ \text{mm}$ for a $26\ \mu\text{m}$ capillary to be
51 approximately $180\ \mu\text{m}$ and therefore $200\ \mu\text{m} \times 200\ \mu\text{m}$ pixels were chosen. However, the spatial resolution obtainable with
52 such irregularly shaped specimens (in all three spatial dimensions) is unlikely to be the same as that observed when using
53 planar substrates.
54

55
56 Fig. 5b is a positive ion mass spectral image of the seeds displayed in Fig. 5a obtained using a $26\ \mu\text{m}$ diameter
57 capillary. A typical positive ion mass spectrum of the seeds is displayed in the *SI* (Fig. S4). Fig. 5b is constructed using the
58 same software packages as outlined earlier and uses the variation in intensity of the positive ion located at $m/z\ 81$. This
59 image clearly depicts the cardamom seeds as shown in Fig. 5a and also shows an apparent distribution of this ion, with two
60

1
2
3 circular areas coloured in red, common to both seeds. It is clear however that the spatial resolution of the device is lower
4 than that achieved with planar substrates.
5

6 GC-MS studies of the essential oil of cardamom seeds report that 1,8-cineole, $M = 154.1357$, constitutes anything
7 from 43 – 89% of the dried capsules.⁴³⁻⁴⁵ The positive ion located at m/z 81 could therefore be the protonated cyclohexane
8 fragment of 1,8-cineole $[M+H-3(CH_3)-COH]^+$. Unfortunately MS/MS was not conducted on the ion fragments in order to
9 substantiate an unambiguous identification. A further positive ion image of m/z 95 can also be seen in Fig. S5. Again, one
10 possible assignment of this ion is to a different fragment of 1,8-cineole $[M+H-C(CH_3)(CH_3)-H_2O]^+$, where VOCs, aromatic
11 molecules which readily interact with the plasma/air mixture, result in higher levels of fragmentation but this cannot be
12 confirmed without further data.
13
14

15 Also displayed in the *SI* (Fig. S6) are positive ion mass spectra taken from the mass spectral image of four
16 different ions observed in Fig. S4: (a) m/z 137 and 155 (inset) and (b) m/z 81 and 95. A close inspection of Fig. S6 shows
17 that the ions located at m/z 137 and 155, which could be associated with the loss of water from protonated 1,8-cineole and
18 the protonated molecule itself respectively, share the same mass spectral profile as ambient ions generated by plasma air
19 interactions. This is in contrast to the ions located at m/z 81 and 95, which clearly originate from the right hand seed and
20 show a mass profile distinct from that generated by plasma/air interactions.
21
22

23 It is likely that the irregular, non-symmetrical and uneven substrates presented to the plasma plume create fluid
24 dynamic distortions both at the centre of the seed and at the edges. Of course, this will impact on image quality and the
25 intensity profiles produced in a complex fashion. A full analysis of plasma interactions at the surface and edges of the seed is
26 beyond the scope of this investigation.
27
28
29
30
31
32
33
34
35
36
37
38
39
40
41
42
43
44
45
46
47
48
49
50
51
52
53
54
55
56
57
58
59
60

Conclusions

This study used a model sample of PTFE wrapped around glass microscope slides to study the effects of principal parameters on the spectral intensity and spatial resolution of ambient MS images. In order to obtain the maximum spatial resolution achieved with this device, $147 \pm 28 \mu\text{m}$, recommended values of these parameters are $1 \text{ mm} \leq z \leq 2 \text{ mm}$, $1.5 \text{ mm} \leq r \leq 2 \text{ mm}$, $D_c = 20 \mu\text{m}$ and source flow rate $\geq 40 \text{ ml/min}$ for this experimental system. It is clear the major factors affecting signal and spatial resolution are the diameter of and the flow rate through the capillary. The spatial resolution achieved with this micro-plasma is in the realm of other ambient mass spectrometry imaging techniques and could be improved with further modifications to the system.

The RSD of signal intensities is found to be approximately 2.3 – 6.5% and which originate from the plasma source rather than the mass spectrometer. This is significantly better than that reported previously with both PADI and conventional LTP itself.

These studies were also able to observe and detect non-volatiles even at non-thermal operating temperatures, thereby limiting damage to sensitive surfaces. These investigations provide evidence of significant advantages of the micro-plasma device. These can be summarised as the absence of sample preparation, inexpensive construction, improved signal stability, detection and simple identification of a range of both volatile and non-volatile compounds and the ability to image real-world foodstuffs. Such strengths offer the potential ability to conduct MS imaging of more complicated samples in a rapid and efficient manner.

Acknowledgements

The authors would like to thank The Engineering and Physical Sciences Research Council (EPSRC) and the Chemical and Biological Programme of the National Measurement System of the UK Department of Business, Innovation and Skills for financially supporting this work. The authors thank Dr. Melissa K. Passarelli for discussions on mass spectrometry analysis and Mr. Alan Roby for constructing the plasma device.

References

(a) Department of Electrical Engineering and Electronics, University of Liverpool, L69 3GJ, UK. Tel: +44 (0) 151 794 4593; E-mail: a.bowfield@liv.ac.uk

(b) National Physical Laboratory, Teddington, Middlesex, TW11 0LW, UK

(c) Centre for Analytical Bioscience and Laboratory of Biophysics and Surface Analysis School of Pharmacy, University of Nottingham, NG7 2RD, UK

- (1) M. E. Monge, G. A. Harris, P. Dwivedi and F. M. Fernández, *Chem. Rev.* 2013, **113**, 2269.
- (2) G. A. Harris, A. S. Galhena and F. M. Fernández, *Anal. Chem.* 2011, **83**, 4508.
- (3) J. P. Williams, V. J. Patel, R. Holland and J. H. Scrivens, *Rapid Comm. Mass Spec.* 2006, **20**, 1447.
- (4) A. Bowfield, D. A. Barrett, M. R. Alexander, C. A. Ortori, F. M. Rutten, T. L. Salter, I. S. Gilmore and J. W. Bradley, *Rev. Sci. Instrum.* 2012, **83**, 063503.
- (5) T. L. Salter, I. S. Gilmore, A. Bowfield, O. T. Olabanji and J. W. Bradley, *Anal. Chem.* 2013, **85**, 1675.
- (6) M. J. Stein, E. Lo, D. G. Castner and B. D. Ratner, *Anal. Chem.* 2012, **84**, 1572.
- (7) A. U. Jackson, J. F. García-Reyes, J. D. Harper, J. S. Wiley, A. Molina-Díaz, Z. Ouyang and R. G. Cooks, *Analyst* 2010, **135**, 927.
- (8) J. S. Wiley, J. F. García-Reyes, J. D. Harper, N. A. Charipar, Z. Ouyang and R. G. Cooks, *Analyst* 2010, **135**, 971.
- (9) T. L. Salter, F. M. Green, N. Faruqui and I. S. Gilmore, *Analyst* 2011, **136**, 3274.
- (10) Z. Takats, J. M. Wiseman, B. Gologan and R. G. Cooks, *Science* 2004, **306**, 471.
- (11) X. Ding and Y. Duan, *Mass Spectrom. Rev.* 2013, DOI: 10.1002/mas.21415.
- (12) R. B. Cody, J. A. Laramee and H. D. Durst, *Anal. Chem.* 2005, **77**, 2297.
- (13) N. Na, M. X. Zhao, S. C. Zhang, C. D. Yang and X. R. Zhang, *J. Am. Soc. Mass Spectrom.* 2007, **18**, 1859.
- (14) J. D. Harper, N. A. Charipar, C. C. Mulligan, X. R. Zhang, R. G. Cooks and Z. Ouyang, *Anal. Chem.* 2008, **80**, 9097.
- (15) S. Soparawalla, F. K. Tadjimukhamedov, J. S. Wiley, Z. Ouyang and R. G. Cooks, *Analyst* 2011, **136**, 4392.
- (16) J. S. Wiley, J. T. Shelley and R. G. Cooks, *Anal. Chem.* 2013, **85**, 6545.
- (17) L. V. Ratcliffe, F. J. M. Rutten, D. A. Barrett, T. Whitmore, D. Seymour, C. Greenwood, Y. Aranda-Gonzalvo, S. Robinson and M. McCoustra, *Anal. Chem.* 2007, **79**, 6094.
- (18) G. C. Y. Chan, J. T. Shelley, A. U. Jackson, J. S. Wiley, C. Engelhard, R. G. Cooks and G. M. Hieftje, *J. Anal. At. Spectrom.* 2011, **26**, 1434.
- (19) G. C. Y. Chan, J. T. Shelley, J. S. Wiley, C. Engelhard, A. U. Jackson, R. G. Cooks and G. M. Hieftje, *Anal. Chem.* 2011, **83**, 3675.
- (20) M. S. Heywood, N. Taylor and P. B. Farnsworth, *Anal. Chem.* 2011, **83**, 6493.
- (21) J. T. Shelley, G. C. Y. Chan and G. M. Hieftje, *J. Am. Soc. Mass Spectrom.* 2012, **23**, 407.
- (22) K. McKay, T. L. Salter, A. Bowfield, J. L. Walsh, I. S. Gilmore and J. W. Bradley, *J. Am. Soc. Mass Spectrom.* (Accepted).
- (23) J. Kratzer, Z. Mester and R. E. Sturgeon, *Spectrochim. Acta Pt. B* 2011, **66**, 594.
- (24) M. Teschke, J. Kedzierski, E. G. Finantu-Dinu, D. Korzec and J. Engemann, *IEEE Trans. Plasma Sci.* 2005, **33**, 310.
- (25) J.-S. Oh, O. T. Olabanji, C. Hale, R. Mariani, K. Kontis and J. W. Bradley, *J. Phys. D: Appl. Phys.* 2011, **44**, 155206.
- (26) J.-S. Oh, Y. Aranda-Gonzalvo and J. W. Bradley, *J. Phys. D: Appl. Phys.* 2011, **44**, 365202.
- (27) D. I. Campbell, C. R. Ferreira, L. S. Eberlin and R. G. Cooks, *Anal. Bioanal. Chem.* 2012, **404**, 389.
- (28) Y. Liu, X. Ma, Z. Lin, M. He, G. Han, C. Yang, Z. Xing, S. Zhang and X. Zhang, *Angew. Chem. Int. Ed.* 2010, **49**, 4435.
- (29) S. Martínez-Jarquín and R. Winkler, *Rapid Comm. Mass Spec.* 2013, **27**, 629.
- (30) D. I. Campbell, J. K. Dalgleish, I. Cotte-Rodriguez, S. Maen and R. G. Cooks, *Rapid Comm. Mass Spec.* 2013, **27**, 1828.
- (31) Z. Xing, J. Wang, G. Han, B. Kuermaiti, S. Zhang and X. Zhang, *Anal. Chem.* 2010, **82**, 5872.
- (32) A. Römpf and B. Spengler, *Histochem. Cell Biol.* 2013, **139**, 759.
- (33) A. Zavalin, E. M. Todd, P. D. Rawhouser, J. Yang, J. L. Norris and R. M. Caprioli, *J. Mass Spectrom.* 2012, **47**, 1473.
- (34) F. Kollmer, W. Paul, M. Krehl and E. Niehuis, *Surf. Interface Anal.* 2013, **45**, 312.
- (35) J. T. Shelley, S. J. Ray and G. M. Hieftje, *Anal. Chem.* 2008, **80**, 8308.
- (36) H. A. O. Wang, D. Grolimund, C. Giesen, C. N. Borca, J. R. H. Shaw-Stewart, B. Bodenmiller and D. Günther, *Anal. Chem.* 2013, **85**, 10107.
- (37) Y. Liu, Z. Lin, S. Zhang, C. Yang and X. Zhang, *Anal. Bioanal. Chem.* 2009, **395**, 591.

- 1
2
3 (38) H. Ayan, E. D. Yildirim, D. D. Pappas and W. Sun, *Appl. Phys. Lett.* 2011, **99**, 111502.
4 (39) M. C. Chambers, B. Maclean, R. Burke, D. Amodei, D. L. Ruderman, *et al. Nat. Biotechnol.* 2012, **30**, 918.
5 (40) A. M. Race, I. B. Styles and J. Bunch, *J. Proteom.* 2012, **75**, 5111.
6 (41) M. P. Seah, *Surf. Interface Anal.* 2002, **33**, 950.
7 (42) J. I. Zhang, A. B. Costa, W. A. Tao and R. G. Cooks, *Analyst* 2011, **136**, 3091.
8 (43) J. I. Zhang, W. A. Tao and R. G. Cooks, *Anal. Chem.* 2011, **83**, 4738.
9 (43) R. Kakei, A. Ogino, F. Iwata and M. Nagatsu, *Thin Solid Films* 2010, **518**, 3457.
10
11
12 (43) A. K. Bhandari, V. K. Bisht, J. S. Negi and M. Baunthiya, *J. Med. Plants Res.* 2013, **7**, 1957.
13 (44) R. Joshi, P. Sharma, V. Sharma, R. Prasad, R. K. Sud and A. Gulati, *J. Sci. Food Agric.* 2013, **93**, 1303.
14 (45) I. P. S. Kapoor, B. Singh, G. Singh, V. Isidorov and L. Szczepaniak, *Int. J. Ess. Oil. Ther.* 2008, **2**, 29.
15
16
17
18
19
20
21
22
23
24
25
26
27
28
29
30
31
32
33
34
35
36
37
38
39
40
41
42
43
44
45
46
47
48
49
50
51
52
53
54
55
56
57
58
59
60

Figures

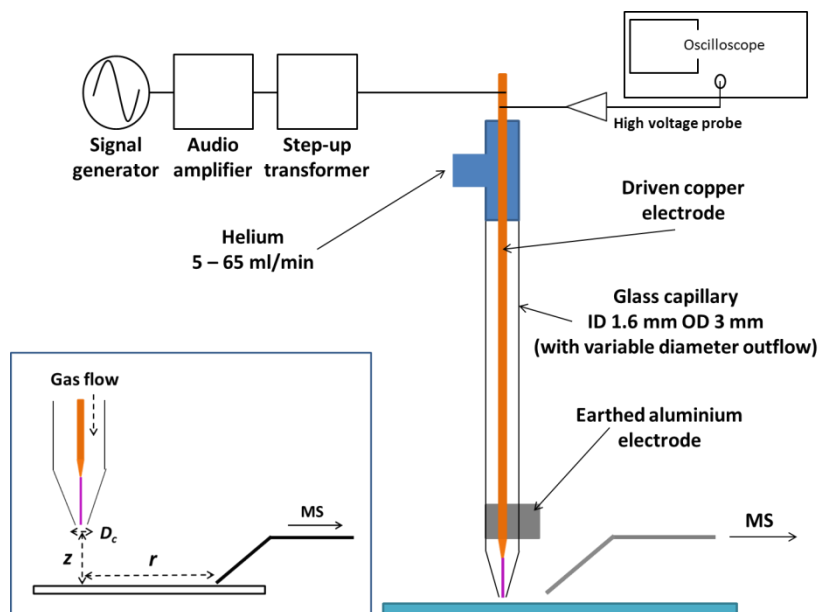


Fig. 1 A schematic of the plasma device with labelled components. The inset also shows the different parameters varied in this study. An optical image of the device in operation is included in *SI* (Fig. S2).

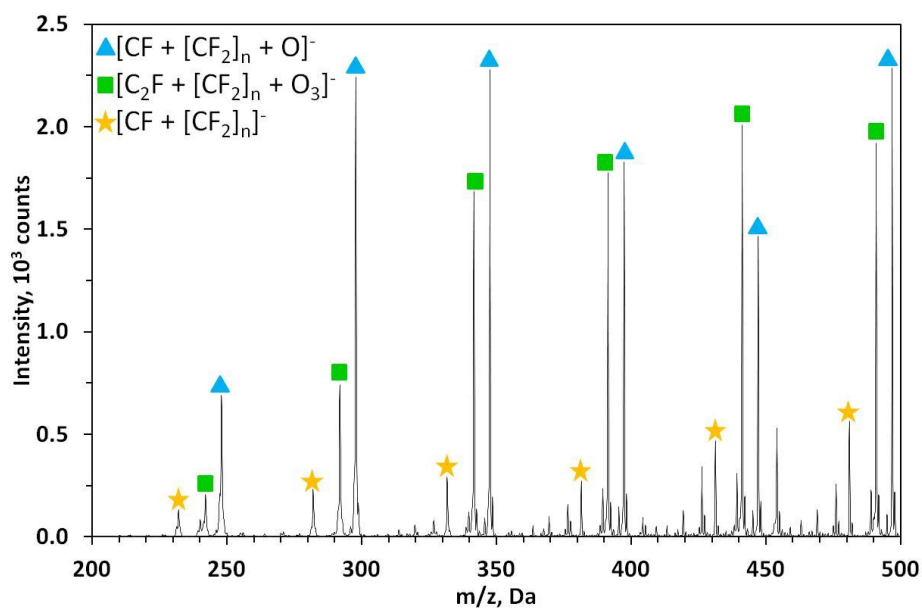
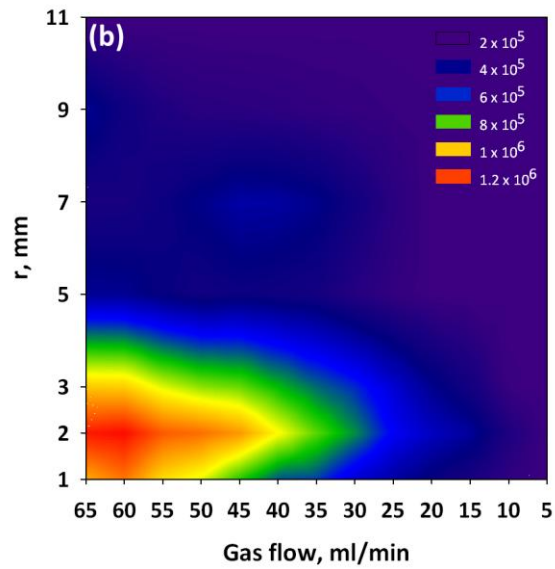
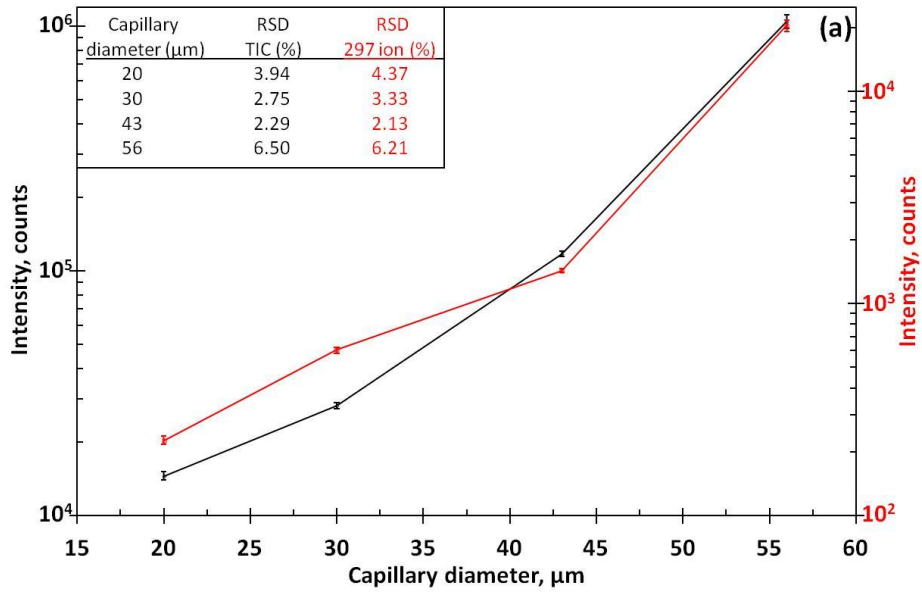


Fig. 2 A typical negative ion mass spectrum of the PTFE substrate in the m/z 200 – 500 spectral window. The three major ion series are labelled using the same icons from a previous investigation⁵ and are identified in the legend in the top left hand corner.



Analyst Accepted Manuscript

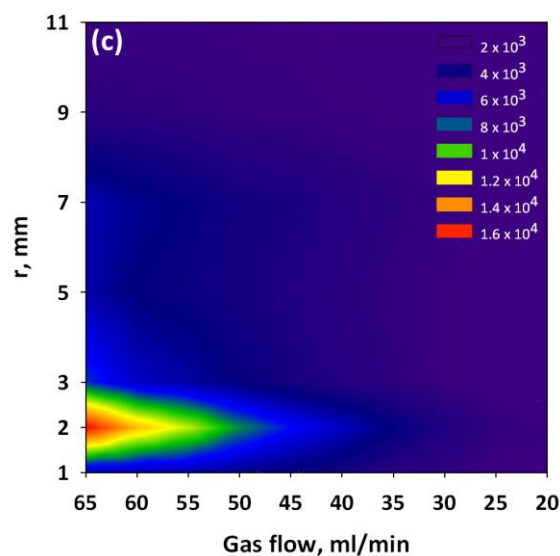


Fig. 3 (a) Variation of average TIC (black line, left hand axis) and peak intensity of the m/z 297 ion from PTFE (red line, right hand axis) as a function of capillary diameter at 65 ml/min. A Log scale is used on both axes for visualisation purposes. Note the approximately exponentially proportional relationship between signal and capillary diameter. The inset displays the relative standard deviation in signal (%) of each capillary for both TIC and the m/z 297 ion. 2D contour maps to show the average TIC as a function of gas flow for each value of r for (b) 56 μm and (c) 20 μm diameter capillaries at $z = 1$ mm. The different colours represent intensity intervals (counts) as described by the legend on the top right of each graph.

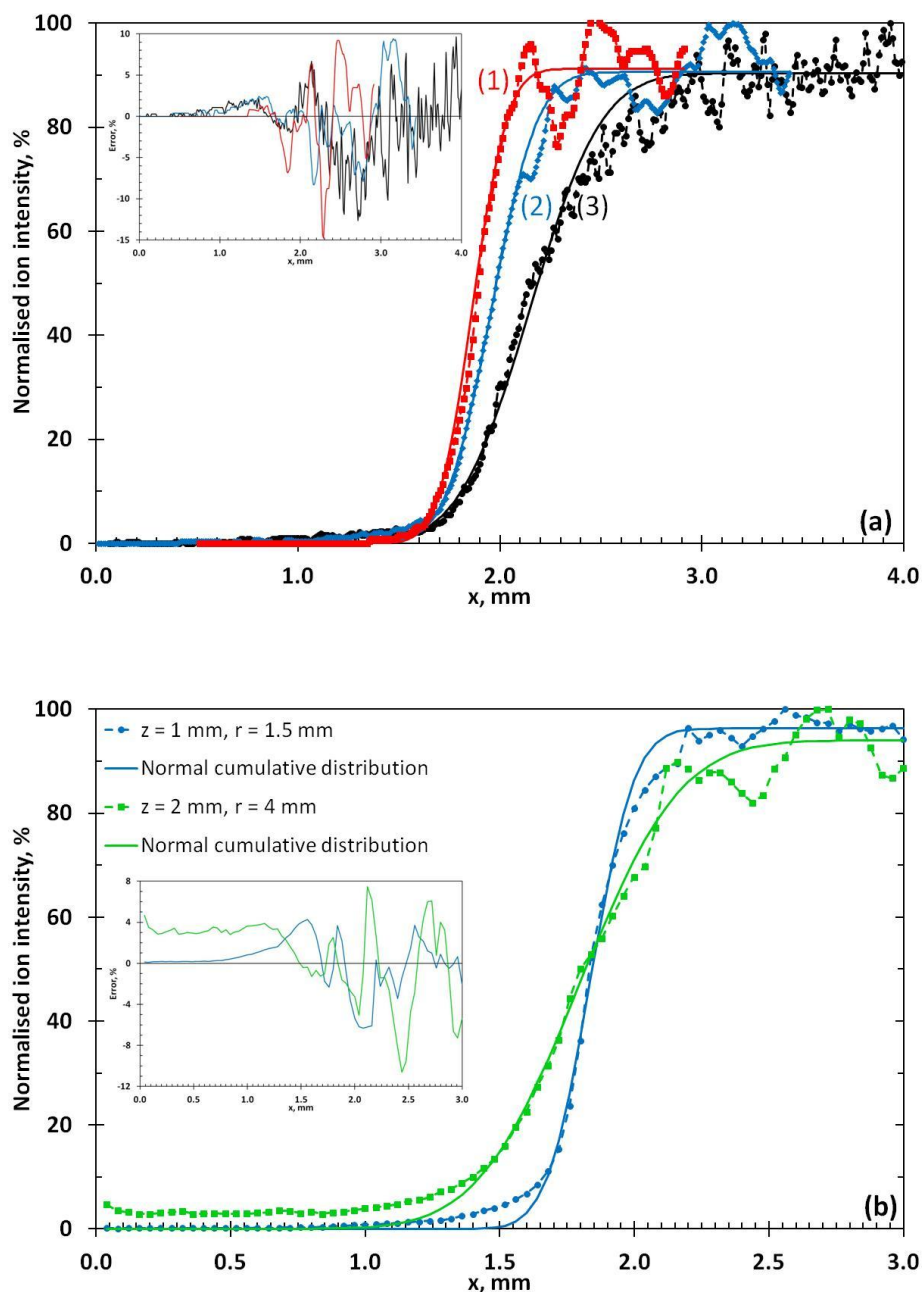


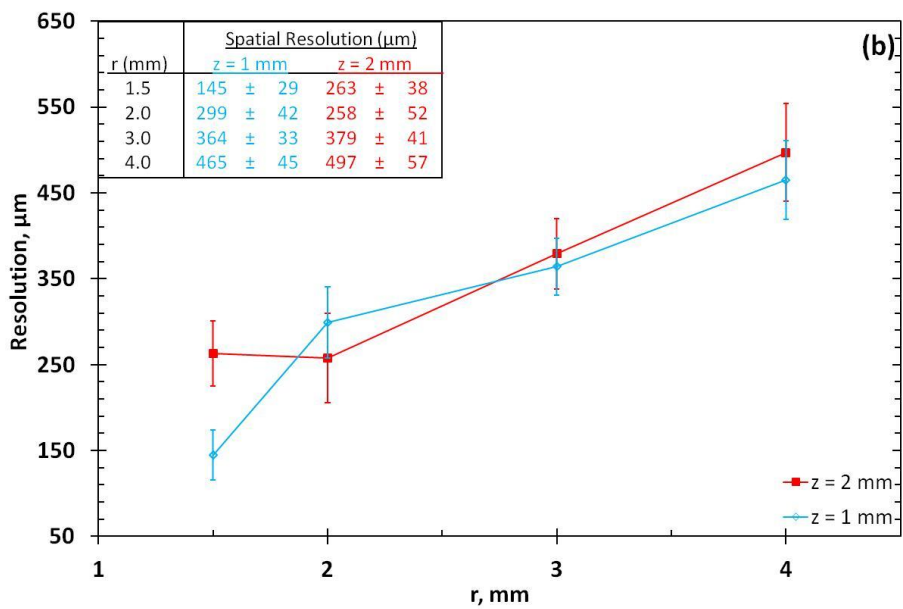
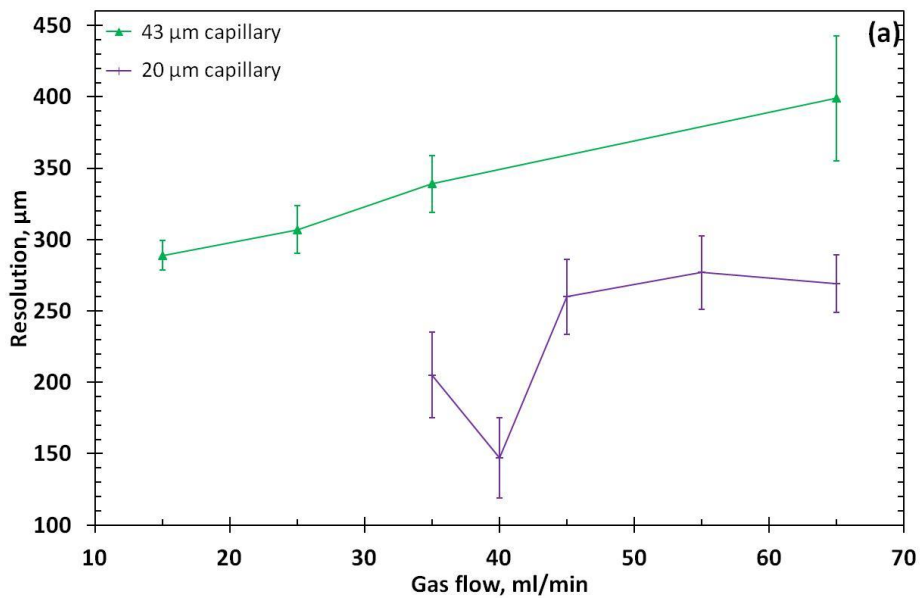
Fig. 4 (a) Line profile of the intensity variation of the m/z 297 PTFE ion across a step edge for (1) 30 μm , (2) 43 μm and (3) 56 μm diameter capillaries at 65 ml/min with $z = 1$ mm, $r = 1.5$ mm. Individual data points for each of the 443 averaged pixels (filled shapes) are included, as well as normal cumulative distribution fits to the experimental data. The inset displays the subtraction of the model from the data. (b) Line profiles of the intensity variation of the m/z 297 ion across a PTFE step edge for a 22 μm diameter capillary at 65 ml/min with $z = 1$ mm, $r = 1.5$ mm (dashed line) and $z = 2$ mm, $r = 4$ mm (solid line). Normal cumulative distribution fits are also included as well as the subtraction of the model from the data (inset).

Table 1. A table to show the source flow rate and spatial resolution of the line profiles contained in Fig. 4(a). Also shown is the standard deviation of each of the normal cumulative distribution fits.

(a)	Capillary diameter (μm)	Source flow rate (ml/min)	σ (μm)	Resolution (μm)
(1)	30	40	98	230
(2)	43	35	147	346
(3)	56	25	234	550

Table 2. A table to show the spatial resolutions of the line profiles contained in Fig. 4(b). Also shown is the standard deviation of both the normal cumulative distribution fits.

(b)	Capillary diameter (μm)	Source flow rate (ml/min)	σ (μm)	Resolution (μm)
$r = 1.5$ mm	22	65	62	145
$r = 4.0$ mm	22	65	211	497



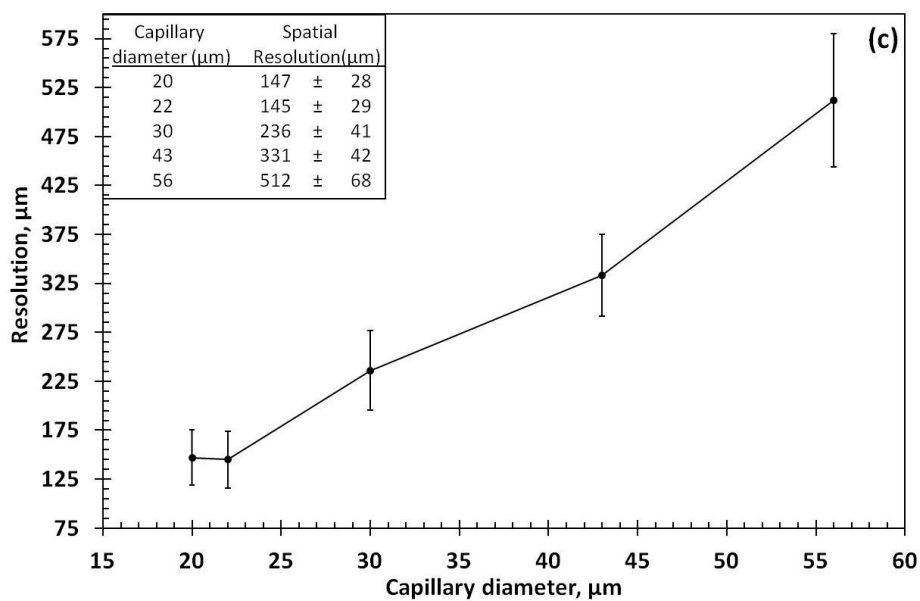


Fig. 5 Variation of spatial resolution as a function of (a) gas flow for two different diameter capillaries at $r = 2$ mm and $z = 1.5$ mm, and (b) r and z for a 20 μm diameter capillary at 65 ml/min. (c) Plot of the spatial resolution achieved with each capillary, displaying an approximately linearly proportional relationship between the two.

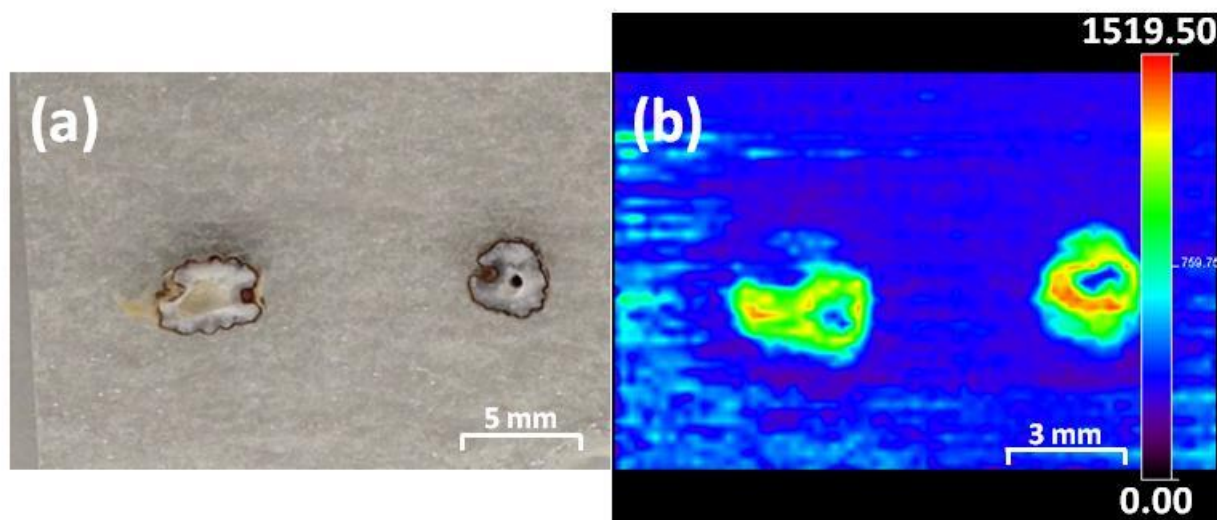


Fig. 6 (a) An optical image of two halves of different cardamom seeds. (b) Positive ion MS image of the seeds shown in (a) using the variation in intensity (counts) of the ion at m/z 81, displayed by the scale bar on the right hand side.